Title

NELL-1 Injection Maintains Long Bone Quantity and Quality in Ovariectomy-Induced Osteoporotic Senile Rat Model

Author

KWAK, JIN HEE

Publication Date

2012

Peer reviewed|Thesis/dissertation

UNIVERSITY OF CALIFORNIA

Los Angeles

NELL-1 Injection Maintains Long Bone Quantity and Quality in Ovariectomy-Induced Osteoporotic Senile Rat Model

A thesis submitted in partial satisfaction

of the requirements for the degree Master of Science

in Oral Biology

by

Jin Hee Kwak

2012

ABSTRACT OF THE THESIS

NELL-1 Injection Maintains Long Bone Quantity and Quality in Ovariectomy-Induced Osteoporotic Senile Rat Model

by

Jin Hee Kwak

Master of Science in Oral Biology

University of California, Los Angeles, 2012

Professor Kang Ting, Chair

Over 10 million Americans have osteoporosis, and is the predominant cause of fractures in the elderly. Treatment of fractures in the setting of osteoporosis is complicated by a suboptimal bone regenerative response due to a decline in the number of osteoblasts, their function and survival. Consequently, an osteogenic therapeutic to prevent and treat fractures in osteoporotic patients is needed. NELL-1 (Nel-like molecule-1), a novel osteoinductive growth factor, has been shown to promote bone regeneration. In this study, we aim to demonstrate the capacity of recombinant NELL-1 to prevent ovariectomy (OVX)-induced osteoporosis in a senile rat model. Ten month old female Sprague Dawley rats underwent either sham surgery or OVX. Subsequently, 50 uL of 600 ug/ml NELL-1 lyophilized onto 0-50 um tricalcium phosphate

(TCP) carrier was injected into the femoral bone marrow cavity while phosphate buffered saline (PBS) control was injected into the contralateral femur. Our microCT results showed that OVX+PBS/TCP control femurs showed a continuous decrease in bone volume (BV) and bone mineral density (BMD) from 2 to 8 weeks post-OVX. In contrast, OVX+NELL-1/TCP femurs showed resistance to OVX-induced bone resorption showing BV and BMD levels similar to that of SHAM femurs at 8 weeks post-OVX. Histology showed increased endosteal woven bone, as well as decreased adipocytes in the bone marrow of NELL-1 treated femurs compared to control. NELL-1 treated femurs also showed increased immunostaining for bone differentiation markers Osteopontin (OPN) and Osteocalcin (OCN). These findings were validated *in vitro*, in which overexpression of NELL-1 in OVX bone marrow stem cells resulted in increased osteogenic differentiation. Thus, NELL-1 effectively enhances *in situ* osteogenesis in the bone marrow, making it potentially useful in the prevention and treatment of osteoporotic fractures.

Key words: NELL-1, osteoporosis, osteogenesis

The thesis of Jin Hee Kwak is approved.

Robert Chiu

Shen Hu

Tara Aghaloo

Xinli Zhang

Kang Ting, Committee Chair

University of California, Los Angeles

2012

TABLE OF CONTENTS

TABLE OF CONTENTS (CON'T)

TABLE OF CONTENTS (CON'T)

ACKNOWLEDGMENTS

This work has been submitted to Tissue Engineering Part A, by which copyright is reserved. The title and co-authors of the submitted manuscript is as follows:

NELL-1 Injection Maintains Long Bone Quantity and Quality in an Ovariectomy-Induced Osteoporotic Senile Rat Model

Jinny Kwak, DDS,[a,#] Janette N. Zara, MD,[b,c,#] Michael Chiang, BDS,[b] Richard Ngo, [b] Jia Shen, PhD,[d] Aaron W. James, MD,[a] Khoi M Le,[b] Crystal Moon,[b] Xinli Zhang, MD, PhD,[b] Zhongru Gou, PhD,[e] Kang Ting, DMD, DMedSci,*[a,b] Chia Soo, MD*[d]

Co-first authors, * Co-senior authors

[a]Section of Orthodontics School of Dentistry, [b]Dental and Craniofacial Research Institute, [c]Department of Bioengineering, [d]Department of Orthopaedic Surgery, University of California, Los Angeles, Los Angeles, CA 90095, [e]Zhejiang-California International NanoSystems Institute, Zhejiang University, Hangzhou, China.

The authors would like to thank the Translational Pathology Core Laboratory (TPCL) and Surgical Pathology divisions of the UCLA Department of Pathology and Laboratory Medicine for technical assistance with histology. This work was supported by NIH/NIDCR (grants R21 DE0177711-01, DE01607-01, and R01 DE16107-05S1, ARRA Supplement), UC Discovery Grant Bio07-10677, T32 training fellowship (5T32DE007296-14) for Dr. A.W. James, and CIRM Training Grant TG2-01169 for Dr. J. N. Zara.

INTRODUCTION

Non-healing skeletal defects are addressed in over 2.2 million surgical cases worldwide each year, in diverse fields of orthopaedic, neurocranial, plastic, and oral/dental surgery (1, 2). Especially in the rapidly growing geriatric population, higher incidences of pathologic bone fractures are reported in various clinic vignettes ranging from long bone and hip fractures in osteoporotic patients to fractures of thinned mandible body in aged edentulous patients. With less than optimal bone regenerative response to the commonly used autograft and allograft materials, osteoporosis further complicates both the treatment and the prevention of such fractures. Consequently, there is an increasing need for osteogenic adjuncts to treat and/or prevent bone fractures in osteoporotic patients.

The biology of osteoporosis

Osteoporosis is a condition where there is an imbalance of osteoblast and osteoclast activities towards bone resorption in the continuing process of bone remodeling. Although it is a silent disease that frequently goes unrecognized until the first fracture occurs, osteoporosis is the predominant cause of bone fractures in the elderly. It is estimated that more than 10 million Americans have osteoporosis, one out of every two Caucasian women are expected to experience an osteoporosis-related fracture in the course of her lifetime, and one in five men will have a similar fate (3). At moderate risk, most osteoporosis-related fractures occur in post-menopausal women and elderly men. The underlying biologic conditions in these populations include a decline in the number of inherent bone marrow stem cells (BMSCs) and an altered microenvironment from aging that diverts the BMSCs from osteogenic differentiation (4). For this reason, the biologic response to the commonly used bone substitutes are also less than

optimal in such patients, in terms of efficacy and efficiency of bone regeneration and the frequency and magnitude of unwanted side-effects. With the aging global population, the healthcare cost of treating osteoporosis-related fractures is expected to double or triple within the next four decades (5, 6). Consequently, there is an increasing need for improved osteogenic therapeutics to treat and/or prevent bone fractures in osteoporotic patients.

Clinically, osteoporosis is characterized by decreased bone mass and microarchitectural deterioration of bone tissue (7, 8). Based on World Health Organization (WHO) diagnostic classification, osteoporosis is quantitatively diagnosed by dual-energy X-ray absorptiometry (DEXA) measurement of the hip and spine, where the bone mineral density (BMD) is 2.5 standard deviation or more below that of the young adult norm. The pathology is generally divided into two types—rapid loss of bone mass in post-menopausal osteoporosis due to estrogen deficiency, or the more gradual onset senile osteoporosis seen in men and women that occurs with aging (9). Age-related increase in adipogenesis in the bone marrow further leads to decreased osteoblastogenesis (10) as osteoblasts and adipocytes are derived from the same BMSCs. Therefore, there is a natural decline in the number of osteoblasts due to aging, and research have shown a decrease in their function and survival as well (8). For these reasons, the biologic response to even the commonly used bone substitutes are suboptimal in such patients, in terms of efficacy and efficiency of bone regeneration and the frequency and magnitude of unwanted side effects (11). For the same reason, loss of healing capacity also complicates routine medical and dental operations involving bone tissue; with or without administration of anti-osteoporosis medication, literatures report compromised bone healing after fracture repair surgeries (12-15) or dental operations including implant insertion and alveolar bone augmentations (16-20). The use of bone graft materials or growth factors are also compromised

in senile osteoporotic patients as they lack regenerative capacity of intrinsic BMSCs. The chronic use of anti-diabetics or corticosteroid in aged patients is also a commonly noted cause of impaired healing capacity of bone in senile patients (21, 22).

Currently available therapies for osteoporosis

In terms of prevention therapy, parathyroid hormone (PTH) is the sole anabolic therapeutic approved by the Food and Drug Administration (FDA) for osteoporosis treatment, and has been shown to increase the BMSC population post-irradiation. PTH, however, is anabolic only when given intermittently, and its use over 2 years has been shown to cause an increase in the development of bone neoplasms in rats (23). Thus, PTH is limited to only once in a lifetime use and only for a limited duration to temporarily reverse osteopenia, soon after which the osteopenic/osteoporotic condition returns (24). A commonly used anti-resorptive agent, bisphosphonate, inhibits osteoclast activity in osteoporotic patients to prevent further bone loss. However, systemic administration of bisphosphonate is associated with adverse effects, including bowel inflammation and erosion of the esophagus when taken orally; possible osteonecrosis of the jaw (ONJ) following high dose intravenous administration in cancer patients; severe bone, joint, or musculoskeletal pain; and fluctuation in calcium blood levels that may increase risk of cardiovascular events (25). In addition, bisphosphonate is an anti-catabolic agent only, and is not capable of regenerating bone. Therefore, an improved, alternative agent that would help prevent osteoporosis-related fractures without exhibiting unwanted systemic effects would be of tremendous clinical advantage.

In terms of treatment of fractured bones using alternative bone graft material, Bone morphogenetic protein 2 (BMP2), the most widely used FDA approved osteoinductive growth

factor incorporated in the graft material. BMP2 is a member of transforming growth factor beta (TGF-ß) superfamily of proteins and thus a non-specific growth factor that contributes to various growth and developmental processes in the body. This functional heterogeneity of BMP2 is known to contribute to clinical complications such as ectopic bone formation (26) and promotion of adipogenesis leading to cystic bone voids (27-29) that compromise the quality of regenerated bone. Moreover, increased complications has been reported with use of BMP2 in osteoporotic patients, leading experts to suggest avoidance of its use in those with osteoporotic bone disease (11).

Discovery and published findings of Nell-1

Nell-1 (Nel-like molecule-1), a novel osteoinductive growth factor originally identified in craniosynostosis patients, has previously been shown to be effective in bone regeneration in various *in vitro* and *in vivo* studies (30-33). It has been shown to be osteoblast-specific, and importantly, is able to suppress the side effects of cystic bone formation seen in high-dose usage of BMP2 (29). In our preliminary *in vivo* study using an ovariectomy-induced osteoporotic mouse model, NELL-1 also demonstrated successful regeneration of bone 3 months post-ovariectomy when locally injected into femurs of 6-month old mice (Kwak et al, ORS Annual Meeting 2010). These findings suggest a role for NELL-1 for bone regeneration in osteoporotic conditions.

In this study, we aim to demonstrate the capacity of NELL-1 to prevent ovariectomy-induced osteoporosis in a senile rat model. We hypothesize that NELL-1, when injected locally

into the bone marrow space of rat femurs, would effectively potentiate the osteogenic capacity of endogenous BMSCs and endosteal osteoblasts to prevent bone loss.

This study is unique in that it uses ten months old female rats that are considered biologically senile. This helps closely mimic the post-menopausal senile human equivalent, and to critically assess the anti-osteoporotic and pro-osteogenic capacity of Nell-1 protein under a challenging osteoporotic environment. Of note, these animals were previously retired breeders.

This study also conforms to the recent FDA guidelines for osteoporosis studies that recommends that agents be evaluated in two animal species, including the ovariectomized rat and a second higher mammal model (34); this study is the first part of the two studies. Another significance of this study is that it is one of the few post-menopausal osteoporosis studies that used senile rats as was recommended by the review of appropriate animal model for osteoporosis studies (35) and the FDA guidelines (34).

MATERIALS AND METHODS

Experimental groups

Twenty-four 10-month old female Sprague-Dawley rats (Charles River Laboratories, Wilmington, MA) were used. Ten month old animals were used as studies have shown that rats of this strain reach peak bone mass by age 9 months; therefore little to no bone modeling occurs that would confound our findings (36). Animals were randomly assigned to the following groups:

- *SHAM group* as the non-osteoporotic control group. A total of six femurs were obtained from three animals, and were harvested at 8 weeks post-sham operation. No animals underwent injection.
- *Ovariectomy (OVX) group* as the osteoporotic control group. A total of six femurs were obtained from three animals, and were harvested at 8 weeks post-OVX operation. No animals underwent injection.
- *NELL-1 groups* were euthanized at 2, 4, and 8 weeks post-OVX and injection procedures. For each time-point, one femur was injected with tricalcium phosphate (TCP) mixed with phosphate-buffered saline (OVX+PBS/TCP; control), and the contralateral femur was injected with Nell-1 lyophilized to TCP and mixed with PBS (OVX+NELL-1/TCP). A total of six control treated femurs and six NELL-1 treated femurs were obtained from six animals for each time-point.

Whole femurs were harvested for high-resolution microCT, histology, and immunohistochemistry analyses after euthanasia. Rat uteri were also harvest and weighed wet and dry as confirmation of ovariectomy as previously described (37, 38).

Injectate preparation

Beta-tricalcium phosphate (ß-TCP) of 10-50 μm particle-size was used as a carrier to deliver and allow sustained release of NELL-1 as previously described (39). The injectates consisted of 50 ul for each femur of 100 mg/ml ß-TCP with or without 600 μg/ml of recombinant human (rh)NELL-1. The optimal dose of NELL-1 was determined based on our previous intramedullary injection study on healthy rat models (*manuscript in preparation*).

Surgical procedure

Animals were housed in a light- and temperature-controlled environment and given food and water *ad libitum*. All animals were handled in accordance with guidelines of the UCLA Chancellor's Animal Research Committee of the Office for Protection of Research Subjects.

Ovariectomy. Sprague Dawley rats were anesthetized by isoflurane inhalation, and buprenorphine injection was administered prior to surgical incision. For ovariectomy, a 5 mm dorsal incision was made on the flank of each rat between the bottom of the rib cage and the front of the hind limb. The tip of a double sharp iridectomy scissors was inserted through the muscle layer, and the muscle fibers were separated. The ovary was pulled through the incision with a blunt forceps by grasping the fat pad surrounding it. High-temperature surgical cautery (Bovie Medical, Clearwater, FL) was used to resect the ovary and oviduct, and the fat pad was replaced into the body cavity after confirming hemostasis. The skin incision was closed using 4-0 vicryl sutures. The procedure was repeated on the contralateral side.

For sham surgery, the fat pad was pulled through the incision with a blunt forceps following the same steps as above. The fat pad was replaced into the body cavity without

resection of the ovary and oviduct. The skin incision was closed using 4-0 vicryl sutures. The procedure was repeated on the contralateral side.

Intramedullary injection. Knee arthrotomy and intramedullary injection of the femur was performed immediately after OVX. Briefly, a 5 mm longitudinal incision was made along the medial aspect of the quadriceps-patellar complex. The patella was dislocated laterally to expose the intercondylar groove. A 0.9 mm k-wire on a trephine drill was used to create a trephination defect. A 26-gauge needle was inserted through the defect, and 50 uL of NELL-1/TCP injectate was injected into the intramedullary cavity. The trephination was sealed with bone wax after injection. The quadriceps-patellar complex was then repositioned and the medial arthrotomy was carefully repaired with 5-0 vicryl sutures. 50 ul of PBS/TCP as control was injected into the contralateral femur, following the same surgical procedure as above.

Radiographic evaluation

Posteroanterior radiographs were taken pre-operation and at harvest using a high-resolution Faxitron LX-60 Cabinet radiography system at a resolution of 10 lp/mm.

Three-dimensional micro-computed tomography evaluation

Post harvest, whole femurs were scanned using high-resolution microCT (Skyscan 1172, Skyscan) at an image resolution of 27.4 um (50 kV and 201 mA radiation source, using a 0.5 mm aluminum filter), and analyzed using DataViewer, Recon, CTAn, and CTVol softwares provided by the manufacturer. The quantitative and structural parameters follow the nomenclatures described by the American Society for Bone and Mineral Research Nomenclature Committee (40).

Femurs were analyzed in three separate regions—proximal femur (PF), mid-shaft (MS), and distal femur (DF)—to comply with published guidelines and to assess site-specific responses to OVX and treatment (34, 35). For analysis, well-established quantitative and structural microCT parameters, including bone mineral density (BMD), percent bone volume (BV/TV), trabecular number, thickness, and separation (Tb.N, Tb.Th, Tb.S) were measured.

Femurs were first re-oriented to an exact upright position in three planes of space (transaxial, sagittal and coronal) using the DataViewer software. Then the highest point of the growth plate on the vertical axis was noted and used as the baseline level from which to divide the femurs into the three regions. Along the vertical axis, the secondary spongiosa at 1 mm proximal to the growth plate was set as the lower (distal) border of the DF to avoid inclusion of newly formed bone in the rats (35). From this level, DF is designated as the lower 6.4 mm, mid-shaft as the middle 8.2 mm, and PF as the top 6.4 mm of the femur segment analyzed (**Figure 1**). These dimensions were determined by careful analysis of the anatomy of all femur samples and calculation of the average number of slices that could be universally applied to all samples.

In examining the scanned images of whole femurs to standardize the method of analysis, transaxial, sagittal, and coronal sectional microCT images of the right and left femurs of each animal were generated for superimposition (**Figure 2.1-2.3**). Transaxial images were generated at various levels along the vertical axis as shown in **Figure 2.1(A)**. This was to determine the relative expansion or resorption of the periosteal and endosteal bone between the OVX+PBS/TCP control and OVX+NELL-1/TCP femurs, and also to examine the degree of variance between the non-treated right and left femurs of the SHAM and OVX groups. Differential thresholding was used to eliminate newly formed bone for clearer assessment. The right femur in SHAM and OVX, as well as the OVX+NELL-1/TCP femurs at 2, 4, and 8 week

groups were colored red, mirrored horizontally and superimposed on the contralateral side in green using Adobe Photoshop CS4 (**Figure 2.1(B), 2.2, 2.3**). This is similar to the previously published method of cortical bone analysis in OVX rat model by Jee *et al.* (35), where the bones were analyzed in three distinct layers; inner, middle, and outer cortical zones.

For analysis of trabecular bone, regions of interests (ROIs) were drawn to discreetly select trabecular bone only, maintaining approximately 0.25 mm clearance from the endosteal bone surface. For analysis of cortical bone, ROIs were drawn to fit exactly the outer border on the periosteal surface and the inner border on the endosteal surface. **Figure 3** shows demonstration of ROIs drawn for trabecular and cortical bones.

To determine the optimal threshold, two representative femur pairs (based on radiographic findings) were selected from each group. The threshold for trabecular bone was set to 95-255 to match the normal bone structure in the SHAM and OVX+PBS/TCP control femurs and also partly include less mature intramedullary bone. The threshold for cortical bone was set to 150-255 to match the normal bone structure in the SHAM and OVX+PBS/TCP control femurs while excluding the trabecular components, and was re-assessed in other experimental groups. Three-dimensional images were generated to confirm that the optimized thresholds properly represent the bones. The selected thresholds were then applied to all samples in the experiment.

Histological and immunohistochemical analyses

Following microCT analysis, the specimens were decalcified using Cal-Ex solution (Fisher Scientific, Pittsburgh, PA) for 5 to 7 days, washed with running tap water for 3 to 4 hours and then transferred to 75% ethanol solution. The specimens were then processed for paraffin embedding and 5 μm sagittal sections of each specimen were obtained and stained with hematoxylin and eosin (H&E).

For immunohistochemistry, paraffin slices were deparaffinized, dehydrated, rinsed, and incubated with 3% H2O2 for 20 minutes and then blocked with 0.1% bovine serum albumin in phosphate-buffered saline (PBS) for one hour. Primary antibodies including anti-Osteopontin (OPN) and anti-Osteocalcin (OCN) (Santa Cruz Biotechnology, Santa Cruz, CA) at a dilution of 1:100 was added to each section and incubated at 37°C for 1 h and at 4°C overnight. ABC complex (Vector Laboratories, Burlingame, CA) was applied to the sections following the incubation with biotinylated secondary antibody (Dako Corporation, Carpinteria, CA). AEC plus substrate in red color (Dako, Carpinteria, CA) was used as a chromagen, and the sections were counterstained with light Hematoxylin. PBS substituted for the primary anti-body was used as a negative control. Photomicrographs were acquired using an Olympus BX51 microscope and MicroFire digital microscope camera with PictureFrame software (Optronics, Goleta, CA).

Relative intra-marrow adiposity was quantified using Adobe Photoshop. Relative lipid area was quantified using the Magic Wand tool, normalized to total marrow space within 20x magnification histological photomicrographs of the femurs.

In vitro BMSC differentiation studies

Primary rat bone marrow mesenchymal stem cells (BMSCs) were obtained from the femoral marrow cavity of SD rats. BMSCs were obtained by marrow flush either 4 weeks after ovariectomy or from age-matched controls. Passage 2 cells only were used for experiments. Cells were expanded in Dulbecco's Modified Eagle's Medium (DMEM) at 37°C, 5% C02 as previously described (41). For *in vitro* osteogenic differentiation, OVX and control BMSCs were seeded at equal densities (50,000 cells / 12 well plate). After attachment, medium was replaced with osteogenic differentiation medium (ODM). Medium was supplemented either with

adenoviral delivered Nell-1 (AdNell-1) or control adenovirus (AdLacZ) as previously described (42) at an MOI of 1. ODM was replaced every third day. Alkaline phosphatase staining was performed (indicating intermediate osteogenic differentiation) as previously described (43). Alizarin red staining (indicating terminal osteogenic differentiation) was performed as previously described (43). Photographic quantification was performed, assessing the relative intensity of staining by averaging 3 random microscopic fields using the Magic Wand Tool in Adobe Photoshop.

Statistical analysis

For statistical analysis, Student's t-test was performed paired to compare the PBS/TCP control and NELL-1/TCP femurs within the same treatment group (* $p < 0.05$, ** $p < 0.01$), and unpaired to compare two different groups (# $p < 0.05$, ## $p < 0.01$).

RESULTS

Confirmation of rat OVX-induced osteoporosis model

Uteri were weighted one hour (wet weight) and 12 hours (dry weight) post-harvest. There was a statistically significant decline in uterine weight of OVX samples versus SHAM, providing a surrogate marker for estrogen loss and osteoporosis induction (**Figure 4**).

Superimposition findings

Sectional micro-CT images of right and left side femurs of each animal were generated and superimposed to determine the degree of periosteal and endosteal cortical expansion or shrinkage between the PBS/TCP control side and NELL-1/TCP side, and also to examine the variance between the left and right sides in SHAM and OVX groups. From this, the overall size and shape of the right and left sides of the femurs were found to be similar within each animal. Also, together with a process of differential thresholding to eliminate newly formed bone, expansion of marrow space in 8Wk PBS/TCP and 8Wk OVX groups appeared to be from absolute loss of trabecular structure or endosteal woven bone rather than relative apposition of the contralateral side, and constriction of marrow space in 4Wk and 8Wk NELL-1/TCP groups from absolute augmentation of trabecular bone or endosteal woven bone rather than relative resorption of the contralateral side (**Figure 2.1B, 2.2, 2.3**). A cartoon that summarizes the general findings of right and left superimpositions and differential thresholding is shown in **Figure 5**. The region of interests (ROIs) drawn in red are of equal size for comparison, and are similar to the actual ROIs drawn for microCT analysis.

Three-dimensional micro-computed tomography findings

Trabecular Bone. At 2, 4, and 8 week time-points, OVX+NELL-1/TCP femurs had significantly increased trabecular bone compared to OVX+PBS/TCP control femurs that showed progressive loss of bone in the proximal femur (PF) and mid-shaft femur (MS) regions as shown by three dimensional reconstructions in **Figure 1**. Quantitative analysis of femurs showed that bone volume (BV), bone mineral density (BMD), and trabecular thickness and number of OVX+NELL-1/TCP femurs were comparable to that of the SHAM group and significantly increased when compared to the OVX+PBS/TCP control at 8 weeks in the PF and MS regions (*$p < 0.05$, **$p < 0.01$ compared to PBS/TCP control; #p<0.05, ##p<0.01 compared to SHAM) as shown in **Figures 6** and **7**.

Overall, the distal femur (DF) region showed minimal effects of OVX-induced osteoporosis, and also showed the least difference between PBS/TCP and NELL-1/TCP sides. The OVX+NELL-1/TCP femurs, however, did show maintenance of bone over time, whereas OVX+PBS/TCP control femurs showed continuous loss of bone from 2, 4 and 8 weeks in the distal femur.

Cortical Bone. Cortical bone did not show significant difference in BV or BMD between groups (**Figure 8**). This is in accordance with the literature that osteoporosis induced solely by ovariectomy will not produce significant cortical changes in rats until after 6-9 months post-OVX (44) (45).

Histology and immunohistochemistry findings

H&E staining was performed on 2, 4, and 8 week treated femurs, and 8 week SHAM and OVX femurs. At 2 and 4 weeks, OVX+PBS/TCP and OVX+NELL-1/TCP samples showed

similar levels of bone loss, mainly as thinning of trabecular structure (*data not shown*). By 8 weeks, OVX+PBS/TCP control femurs continued to show considerable reduction of lamellar bone, findings which were similar to that of the OVX group. Conversely, OVX+NELL-1/TCP femurs showed recovery of lamellar bone volume, with very evident increase in endosteal woven bone formation comparable to SHAM group (**Figure 9A-H**).

Immunohistochemistry showed significantly increased distribution and enhanced intensity of OPN (**Figure 9I-L**) and OCN (**Figure 9M-P**) immunostaining in the OVX+NELL-1/TCP treated femurs than that of OVX+PBS/TCP and OVX alone controls. Moreover, the positive staining patterns of OPN and OCN appeared to be distinctly different; OPN was expressed predominantly along the active bone formation fronts while the OCN stains relatively mature bone matrix across all the samples. These results indicate that NELL-1 promotes more active woven bone formation and/or remodeling similar to that observed in SHAM control samples.

In addition, relative intra-marrow adiposity quantification of histological images of OVX+PBS/TCP and OVX+NELL-1/TCP femurs at 8 weeks showed statistically significant reduction in lipid area, and thus, adipogenesis in Nell-1 treated femurs (**Figure 10**).

In vitro results

We next sought to confirm these results *in vitro*, examining the effect of adenoviral delivered (Ad)Nell-1 on BMSCs derived from healthy or ovariectomized rats. Osteogenic differentiation was performed and assessed by alkaline phosphatase (ALP) staining to assess early differentiation (**Figure 11A-D**), and alizarin red (AR) staining to assess terminal differentiation (bone nodule formation**, Figure 11E-H**). Quantification was performed by

photographic assessment (**Figure 11I and J**). At baseline, OVX was observed to result in a reduction in osteogenic differentiation by all markers. Among control rBMSCs, AdNell-1 increased osteogenic differentiation by both ALP and AR staining and quantification. This was also observed among OVX rBMSCs, where AdNell-1 increased all markers of osteodifferentiation.

DISCUSSION

In this study, we demonstrated the ability of NELL-1 to prevent osteoporotic bone loss by local intramarrow injection. In the setting of OVX, NELL-1 injection maintained appendicular bone mass, as assessed by radiologic, histologic, and immunohistochemical methods.

Our osteoporotic model was carefully created to limit confounding factors that may affect the findings in this study. At age 9 months or older, Sprague Dawley rats have reached peak bone mass, and no longer undergoes periosteal expansion from growth at the long diaphyses, and any cortical remodeling will take place only on the inner cortical layer/endosteal surface of bone (46, 47). Of note, rats of this strain undergo menopause at 15 to 18 months of age (48, 49). Therefore, 10 months old senile rats were used to undergo ovariectomy to induce osteoporosis.

Special considerations in selection of osteoporosis animal model

A. Modeling vs. Remodeling

It is important to clearly distinguish modeling and remodeling in osteoporosis research as it influences the selection of animal strain, animal age, specific skeletal sites, and also time frame of the study. Modeling is the basic sculpturing of the bone to "grow in size and to shift in space" (5), and mainly occurs during childhood and adolescence. This occurs via formation of new bone at one site (e.g. outer cortical), and removal of old bone from another site (e.g. inner cortical) (50), therefore, not osteoblast/osteoclast-coupled. Remodeling, on the other hand, is an osteoblast/osteoclast-coupled process that occurs at the same site of the bone in order to build new bone to replace old bone that is losing resilience and depleting in mineral storage. The human bone is remodeled throughout life, and becomes dominant after reaching the peak bone mass by the early 20 years of age, and most of the adult skeleton is replaced about every 10 years

(5). Remodeling is also important and is the predominant activity in skeletal repair and maintaining calcium and phosphorus homeostasis.

B. Animal selection

There has been a controversy as to which animal models should be used in osteoporosis studies to adequately obtain results that are applicable to human subjects. Jee et al. (35) and Thompson et al. (34), have reviewed the FDA Guidelines for evaluation of agents used in the treatment or prevention of postmenopausal osteoporosis (1994), and established more refined guidelines. The authors recommended a careful consideration of the following factors:

[1] *Animal selection.* Modeling is the predominant cellular activity in the mouse skeleton, whereas, although site-specific, remodeling is found to be the predominant activity in the rat skeleton. Therefore, it is advised that evaluation of a treatment be performed in senile ovariectomized female rats prior to initiating a clinical trial.

[2] *Animal age*. Rats of age 9 months or older are recommended to use in evaluation of treatment or prevention of osteoporosis, as female rats of this age reached the peak bone mass and can be manipulated to induce postmenopausal osteoporosis. By 10 months of age, the periosteal expansion from growth also ceases at the long bone diaphysis, and any cortical remodeling will then take place on the inner cortical layer (endosteum) (46, 47). Within the time frame of this study, however, no significant changes in the cortical bone are expected to occur, as it has been reported that bone loss in cortical bone begins around 3-9 months post-OVX, depending on the skeletal site (35).

[3] *Proper selection of skeletal site.* The selected sites for analysis were proximal femur (PF), mid-shaft (MS), and distal femur (DF), where cellular activities are reported to be predominantly remodeling as opposed to modeling (35, 46, 47).

[4] *Site specific sampling problem*. Literatures report that the femoral neck shows natural growth (modeling) longitudinally from the epiphyseal plate at the rate of <1um/day, the proximal tibial metaphysis at the rate of 3um/day, and the distal tibial metaphysis growth plate closed by 9 months of age (35). In this study, the secondary spongiosa at one mm away from the growth plate was selected for analysis as was recommended in order to avoid inclusion of new bone formed by natural growth (35).

[5] *The need for proper controls in dealing with growing bone sites.* In this study, internal controls were established by having one side of the femurs as treatment side, and the other side as carrier control side. Both sham and OVX control groups were included and kept for 8 weeks, to compare with 8 weeks Nell-1 group.

[6] *Awareness of shortcomings of using a rat model:* Rodent skeleton lacks Haversian structure and intracortical remodeling activity. Cortical bone loss occurs on the endosteal and develops very slowly (6-9 months post-OVX) if OVX is not reinforced by additional immobilization and dietary restriction (44, 45). Therefore, rats are not the proper animals to study the intracortical remodeling responsive to a treatment, and would require an additional higher mammal animal model to obtain the pertinent information.

[7] *The timing of intervention in relation to the time-point of ovariectomy.* As a prevention therapy, this study performed ovariectomy and intramarrow injections simultaneously at Day 0. As a prevention study, this study demonstrated that Nell-1 maintains the bone level at 2 and 4 weeks and recovers it to sham level by 8 weeks post-OVX, with significantly less adipogenesis compared to the carrier control.

C. Need for superimposition of bones in comparison

In analyzing porous bones such as in senile or ovariectomized animals, the method of selecting out the trabecular bone becomes uneasy. The reason is because they either naturally have or develop during treatment a zone of fused bone between the endosteal cortical bone and the trabecular bone in marrow space. It becomes a question whether the porosity observed within the marrow space is caused by apposition of bone on the endosteal surface, or by resorption of endosteal bone. An example case is demonstrated in **Figure 12(A)**, where the porosity could be seen as a result of either added or loss of bone.. Thus, it is crucial that experiments involving rescue of porous bones include internal control within each animal as shown in **Figure 12(B)** to compare to the treatment side (**Figure 12(A)**). Of note, based on continuous observation of rodent bone in our laboratory, some rodents older than 3 months of age naturally present fused bone between the cortical and trabecular compartments. In **Figure 12(A,B)**, the comparison of cortical bone thickness between the internal control and the treatment side determined that there was actual augmentation of bone in the treatment side. **Figure 12(C, D)** shows different resulting ROIs that would be drawn in case of resorption **(C)** or apposition **(D)**. In summary, a verification of bone apposition or resorption using a high-resolution, measurable images is extremely important and necessary in order to draw a proper region of interest (ROI) for accurate micro-CT analysis.

In case where the internal control side serves as carrier control side (as was in the current study with PBS/TCP control), the verification becomes more complex as both sides of femurs become variables. In order to overcome this problem, superimposition of the femur pairs within each animal was performed in order to verify whether the treatment femur shows absolute apposition, or the control femur shows absolute resorption and therefore presented a relative apposition in the treatment femur.

From the *in vivo* findings, although there was an initial decline in BV and BMD from 2 to 4 weeks post-OVX, by 8 weeks NELL-1/TCP treatment resulted in an increase in bone levels similar to that of SHAM control. These findings were particularly significant in the proximal and mid-shaft regions of the femur. Overall, the distal femur (DF) showed less response to OVX as well as treatment and may be due to the proximity of the DF to the epiphyseal plate. Failure to show statistically significant differences of cortical bone between groups is not surprising as previous studies have shown that osteoporosis induced solely by OVX will not produce significant cortical changes in rats until after 6-9 months post-OVX (44) (45).

At the cellular level, osteoporosis is characterized by increased bone turnover rate, with an imbalance towards osteoclast-mediated bone resorption. NELL-1's capacity to reverse osteoporosis may be due to its modulation of osteoblast, osteoclast, and adipocyte activity. Mechanistically, NELL-1 is a downstream mediator of Runt-related transcription factor 2 (Runx2), the key transcription factor regulating osteogenic differentiation. Runx2 regulates *NELL-1* expression by binding to its promoter region (51). In turn, NELL-1 upregulates Runx2 bioactivity by enhancing its phosphorylation through transient activation of mitogen-activated protein kinase (MAPK) signaling (52), leading to promotion of bone formation. *Nell-1* overexpression has also been shown to partially rescue Runx2 haploinsufficiency (53). In this study, we showed *in vitro* and *in vivo*, NELL-1's capacity to promote osteogenesis.

With particular relevance to osteoporosis, multiple studies have found that BMSCs demonstrate defective or reduced osteogenesis (54-56). Li *et al.* reported that BMSCs obtained from 3 and 6 month old rats showed decreased proliferative and osteogenic potential compared to control BMSCs (57). Our *in vitro* studies showed similar findings in which we showed reduced osteogenesis in OVX BMSCs as compared to control BMSCs. Although the exact

mechanism of this decline is unknown, our studies showed that NELL-1 is able to reverse this effect. Addition of AdNell-1 to OVX BMSCs lead to increased Alkaline phosphatase (ALP) and Alizarin red (AR) staining, to levels comparable to that of control BMSCs that received no NELL-1 treatment.

Our previous studies have shown that NELL-1 stimulation of Runx2 may be through the canonical (β-catenin dependent) Wnt signaling pathway, which is essential for differentiation of progenitor cells into osteoblasts (58, 59). While the mechanisms by which NELL-1 activates canonical Wnt signaling have not been determined, our previous *in vitro* studies showed that NELL-1 significantly induced β-catenin nuclear accumulation in M2-10B4 cells (*JBMR manuscript in revision*). We further confirmed NELL-1's association with Wnt signaling by performing studies co-applying NELL-1 with Wnt inhibitors. Addition of DICKKOPF-1 (DKK-1), a Wnt antagonist, eliminated NELL-1 induced increase in Runx2 expression in M2-10B4 cells (*JBMR manuscript in revision*).

NELL-1 has also been shown to down regulate peroxisome proliferator-activated receptor gamma (PPAR-γ), a transcription factor and master regulator of adipogenesis. This, again, may be mediated through NELL-1 effects on Wnt signaling, as Wnt signaling is known to inhibit PPAR-γ, and subsequently, adipogenesis, in multiple cell lines (60, 61). Indeed, quantification of intra-marrow adiposity of our histological results confirmed decreased adipocyte accumulation in the marrow of OVX+NELL-1/TCP femurs compared to all other groups.

Finally, several lines of evidence suggest that loss of Nell-1 is in fact associated with the development of bone loss and osteoporosis. We previously examined and reported on the skeletal phenotype of mice deficient in Nell-1. In the study, loss of *Nell-1* was produced by E-nitrosourea (ENU) mutagenesis (62), however, complete deficiency in *Nell-1* was shown to be neonatal

lethal. After this finding, we have then examined adult and aged mice heterozyotes for *Nell-1* mutation induced the way say; preliminary results have demonstrated a clear osteopenic / osteoporotic phenotype that develops with age and is most prominent in the thoracic and lumbar spines. In ongoing studies, it appears that this is associated with reduced bone formation, and also inappropriately maintained bone resorption. Our newly discovered osteoporotic, *Nell-1* deficient mouse model also has a human correlate. In a 2010 article, Karasik *et al*. evaluated over 430,000 single nucleotide polymorphisms (SNPs) in over 2000 women in the Framingham Osteoporosis Study (63). *NELL-1* was one of only 10 genes harboring an SNP found to be associated with reduced bone mineral density in the femoral neck and lumbar spine. In aggregate, these observations span both animal research and clinical studies and suggest that loss of NELL-1 function may in fact contribute to the natural development of osteoporosis.

In the context of the present study, these data suggest that NELL-1 may be not only a causative factor, but also a future therapeutic for osteoporotic bone loss. From this and previous studies, we know that NELL-1 increases local bone formation by increasing osteoblast differentiation and activity, but without a concomitant osteoclast response. These qualities make NELL-1 an appealing future therapy used for local application of NELL-1 in the prevention of fragility fractures in high fracture-risk patients. Further studies using higher mammals such as sheep that have similar cortical bone structure as humans, including the Haversian structures, are needed in order to evaluate NELL-1's effects on not only the trabecular, but also the cortical bone.

Clinical advantages of Nell-1

There are several notable advantages of Nell-1 as a new agent for prevention and possibly treatment of osteoporosis and osteoporotic fractures. Nell-1 has demonstrated successful bone formation while inhibiting side-effects of non-specific osteogenic agents such as BMP2 (64). The findings from this and previous studies on Nell-1's effect on healthy and osteoporotic BMSCs also suggest possible use of Nell-1 in both prevention and treatment of postmenopausal osteoporosis. Another key advantage of Nell-1 is its flexibility in the delivery system; it could be delivered through (i) direct delivery of recombinant protein, either mixed in a putty of demineralized bone matrix (DBM) or injected flowable mixed with PBS, or through (ii) viral transfection of the gene, as previously described (39, 65-67).

CONCLUSION

We demonstrated the ability of NELL-1 to successfully prevent the loss of bone volume, bone mineral density, and trabecular microstructure in an OVX-induced osteoporotic senile rat model. Our *in vitro* and *in vivo* findings suggest NELL-1's capacity to harness and further enhance the osteogenic potential of endogenous BMSCs and endosteal osteoblasts in both healthy and osteoporotic bones.

FIGURES

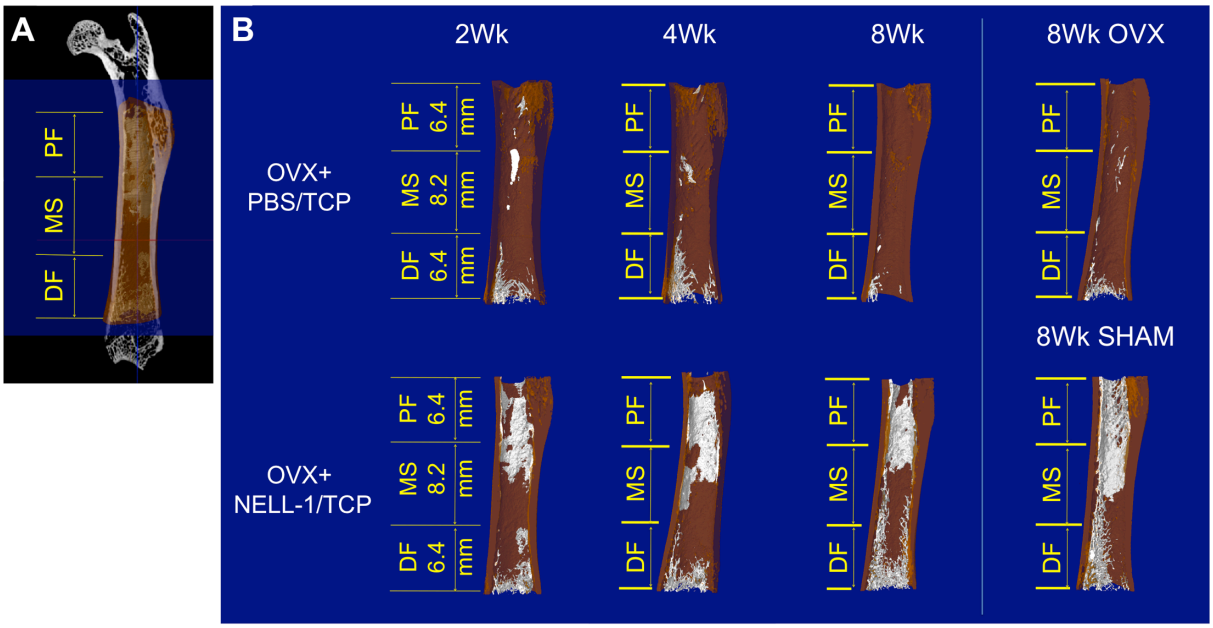

Figure 1. MicroCT 3D reconstructions showing trabecular bone formation. Post-harvest, whole femurs where analyzed using microCT. (**A**) Schematic of femur region designations, defining the proximal (PF), mid-shaft (MS), and distal femur (DF) as analyzed. (**B**) In the proximal femur (PF) and mid-shaft (MS) regions, the OVX+PBS/TCP control samples demonstrated continuous decrease in bone quantity and quality from 2 to 8 weeks, and approached the level of OVX only samples by 8 weeks. In contrast, the OVX+NELL-1/TCP femurs maintained bone levels from 2 to 8 weeks, approaching SHAM levels by 8 weeks. The distal femur (DF) was least affected by either ovariectomy or treatment, with minimal changes in trabecular bone. In order to visualize the inner trabecular bone, the cortical bone was hemi-sectioned coronally in 3D reconstructions.

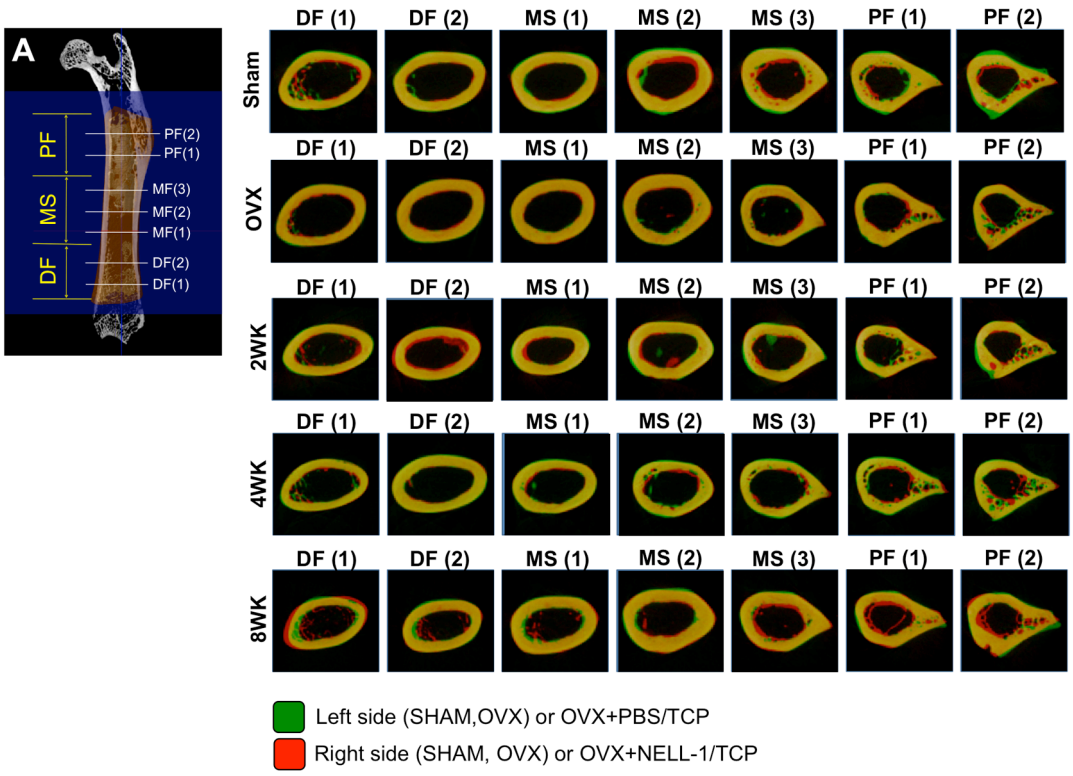

Figure 2.1. Superimposition of femur pairs (microCT). Transaxial view. (A) Femurs were cross-sectioned in constant distances; each of DF, MS, and PF sections were divided into 3, 4 and 3 equal lengths. (B) The image of right side (SHAM,OVX) or NELL-1/TCP side femur in red has been mirrored and superimposed on its contralateral side in green. This was to help determine the relative expansion or shrinkage of the periosteal and endosteal bone between the PBS/TCP control and NELL-1/TCP sides, and also to examine the degree of variance between the non-treated right and left sides of SHAM and OVX groups. Note that the overall size and shape of the two sides of femurs are similar within the same animal. From these findings together with differential thresholdings to eliminate newly formed bone, expansion of marrow space in 8Wk PBS/TCP and 8Wk OVX groups appeared to be from absolute loss of trabecular structure or endosteal woven bone rather than relative apposition of the contralateral side, and constriction of marrow space in 4Wk and 8Wk NELL-1/TCP groups from absolute augmentation

of trabecular bone or endosteal woven bone rather than relative resorption of the contralateral side.

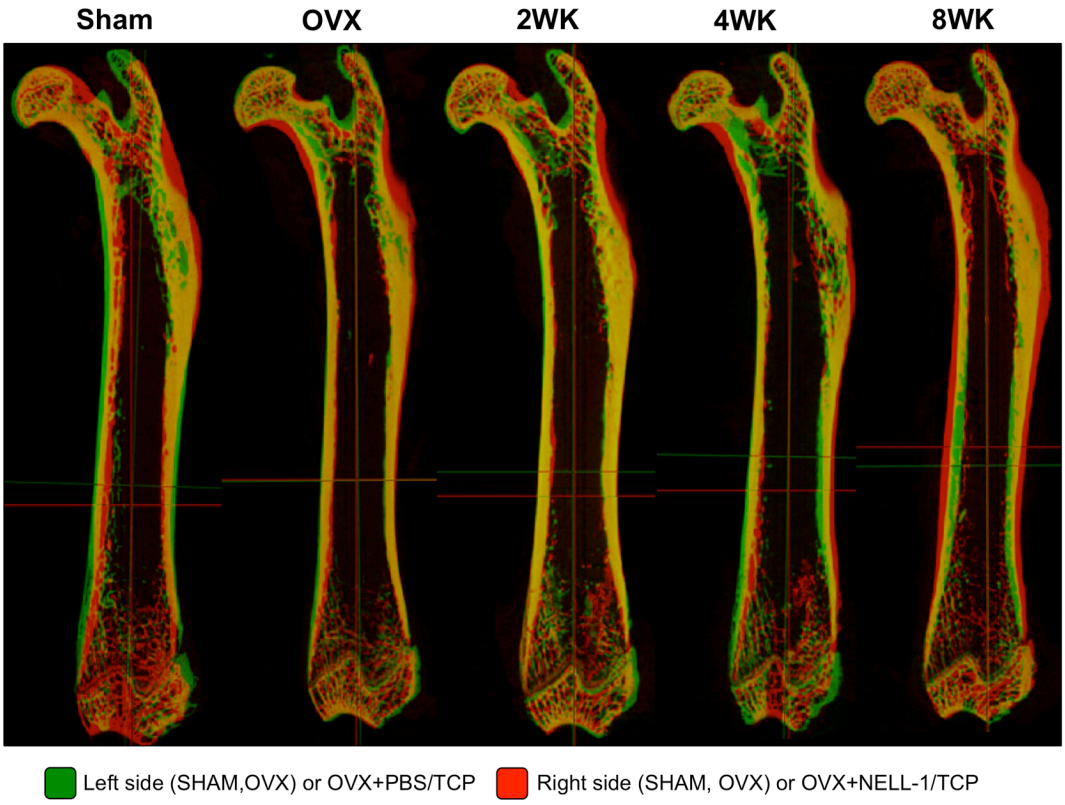

Figure 2.2. Superimposition of femur pairs (microCT). Sagittal view.

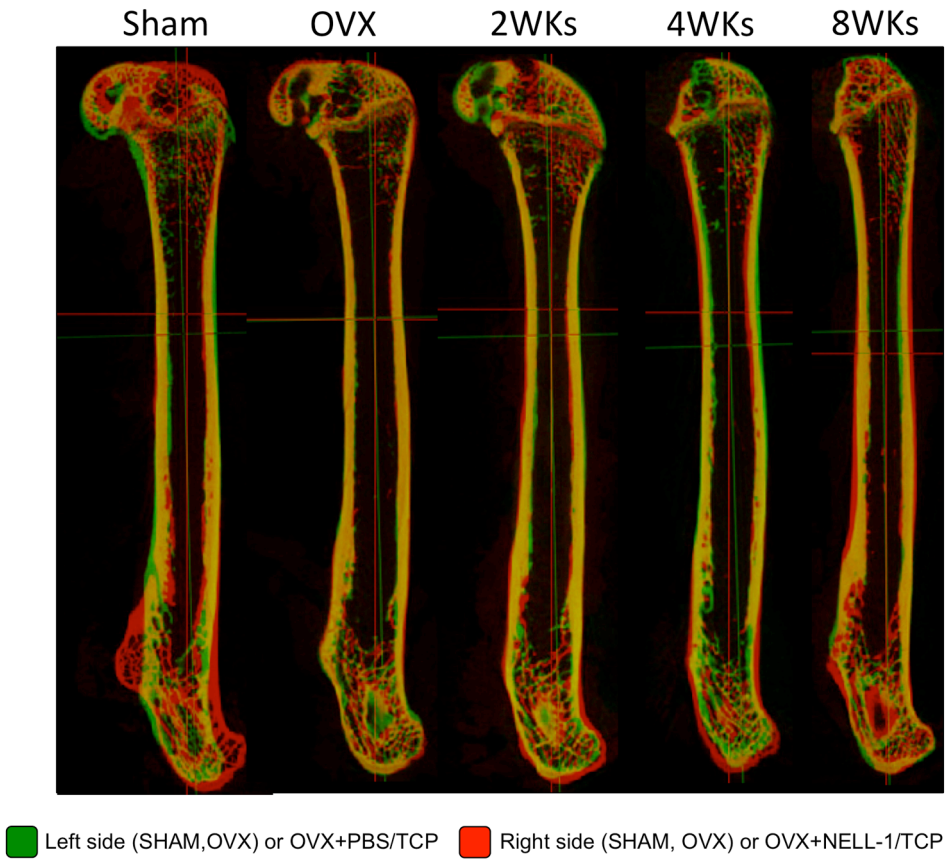

Figure 2.3. Superimposition of femur pairs (microCT). Coronal view.

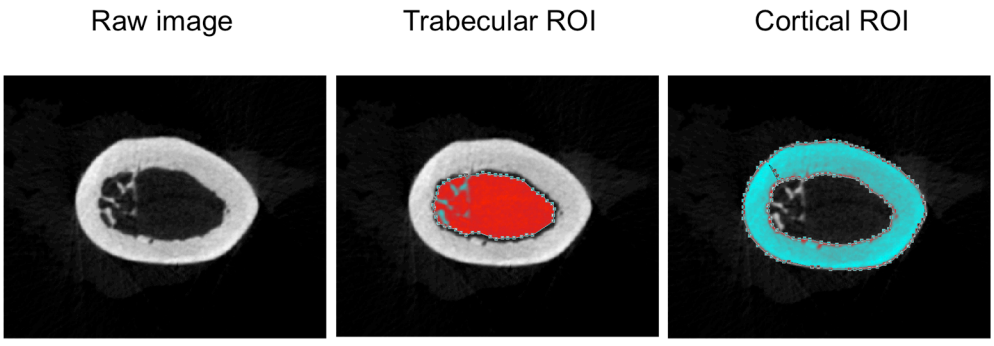

Figure 3. Demonstration of microCT ROIs for trabecular and cortical bones.

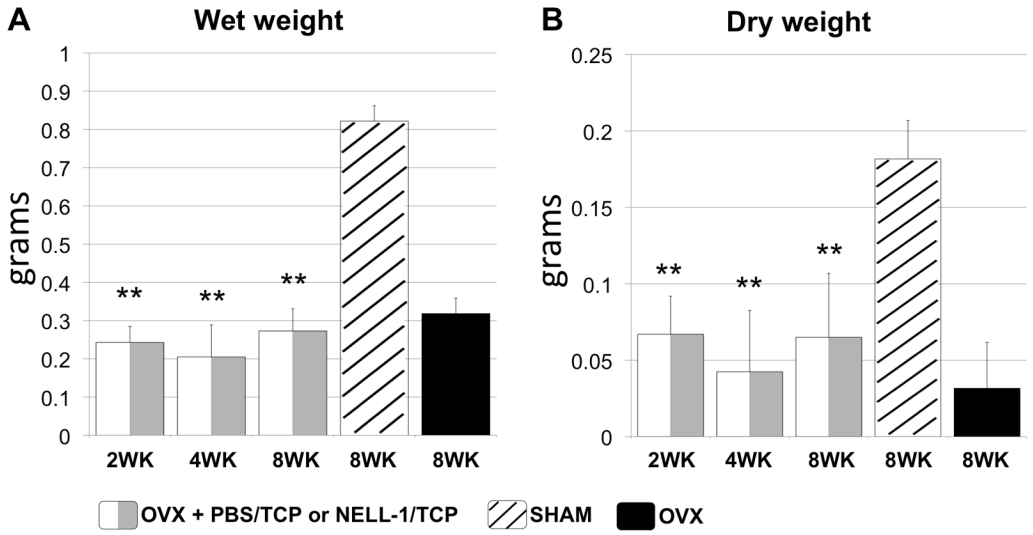

Figure 4. Uteri weight. Uteri weight at (**A**) 1 hr (wet weight) and (**B**) 12 hr (dry weight) showed a statistically significant decrease in OVX samples compared to SHAM. ** $p < 0.01$.

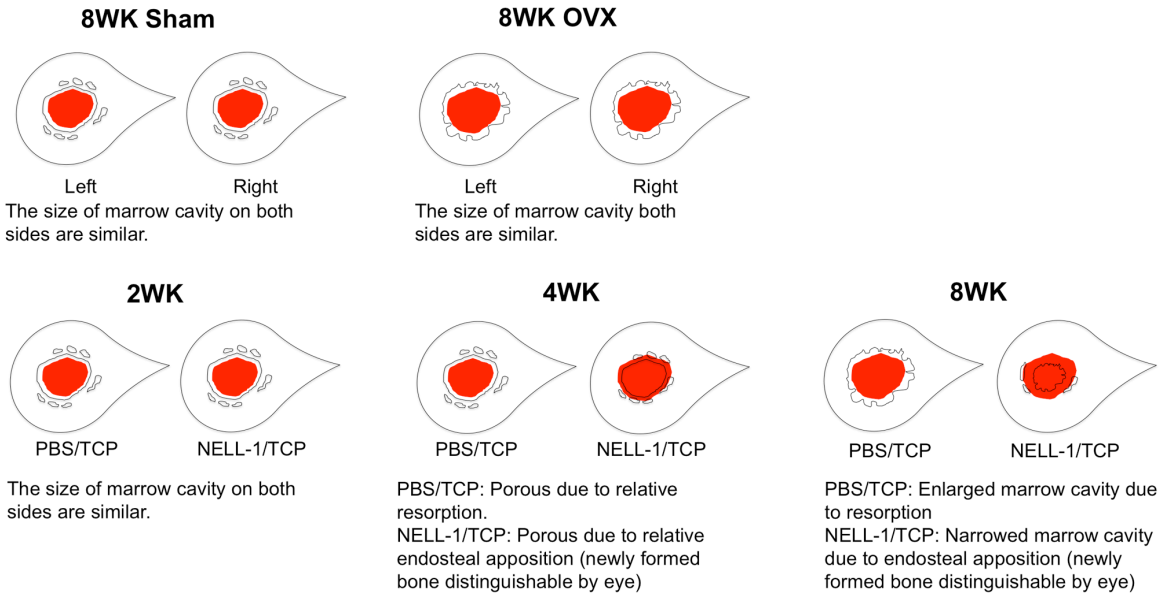

Figure 5. Summary of superimposition findings. The superimposition findings were useful in systemizing both the trabecular analysis (to determine relative apposition or resorption) and the

cortical analysis (to determine expansion or shrinkage of inner and outer cortical borders). The region of interests (ROIs) drawn in red are of equal size for comparison, and are similar to the actual ROIs drawn for micro-CT analysis.

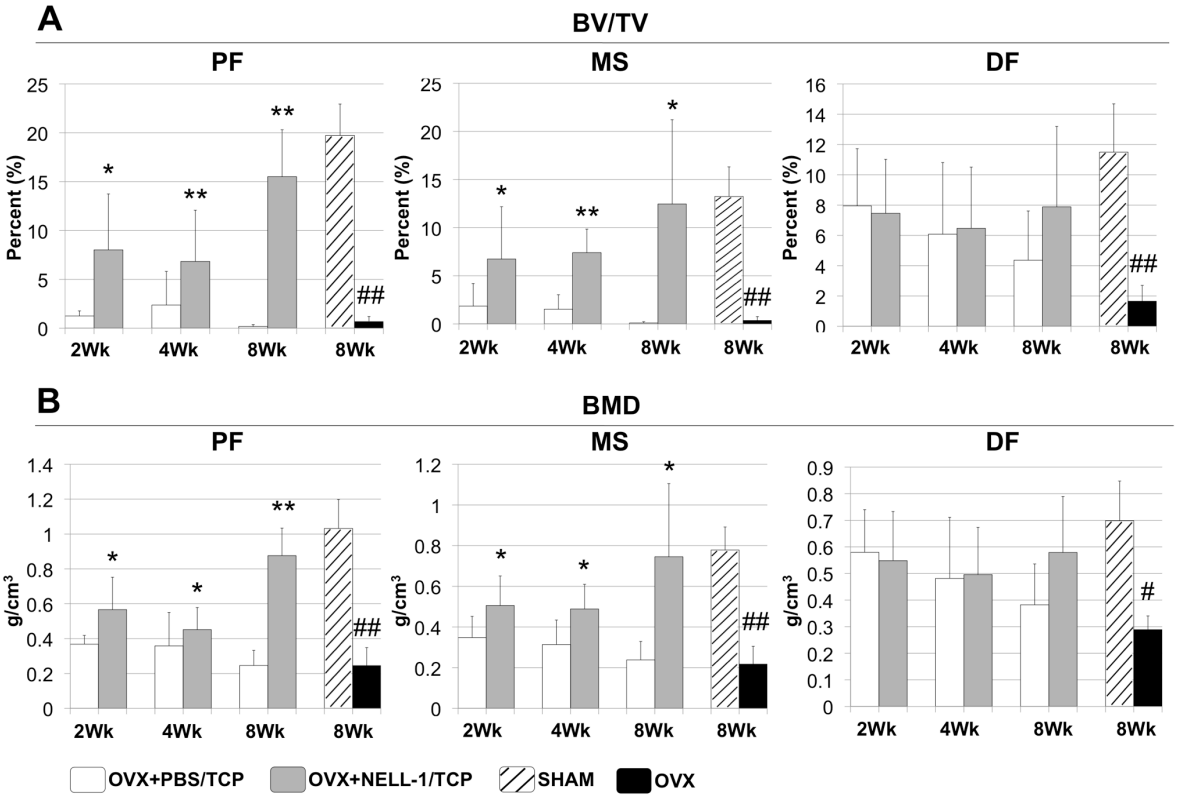

Figure 6. Quantitative microCT analysis of trabecular bone volume and bone mineral density. Trabecular bone was analyzed from the 2, 4, and 8 week OVX+NELL-1/TCP and OVX+PBS/TCP control treated groups, as well as 8 week SHAM and OVX only groups in the PF, MS, and DF segments. (**A**) Analysis of percent bone volume (BV/TV) and **(B)** bone mineral density (BMD). For both BV/TV and BMD, the difference between SHAM and OVX only groups was statistically significant in proximal femur (PF) and mid-shaft (MS) regions, but less in the distal femur (DF) region. Overall, the DF region was least affected by ovariectomy and/or treatment. * $p < 0.05$, ** $p < 0.01$ for paired t-test between PBS/TCP and NELL-1/TCP groups

within each time point; # $p < 0.05$, ## $p < 0.01$ for 1-way, unpaired t-test between SHAM and OVX groups.

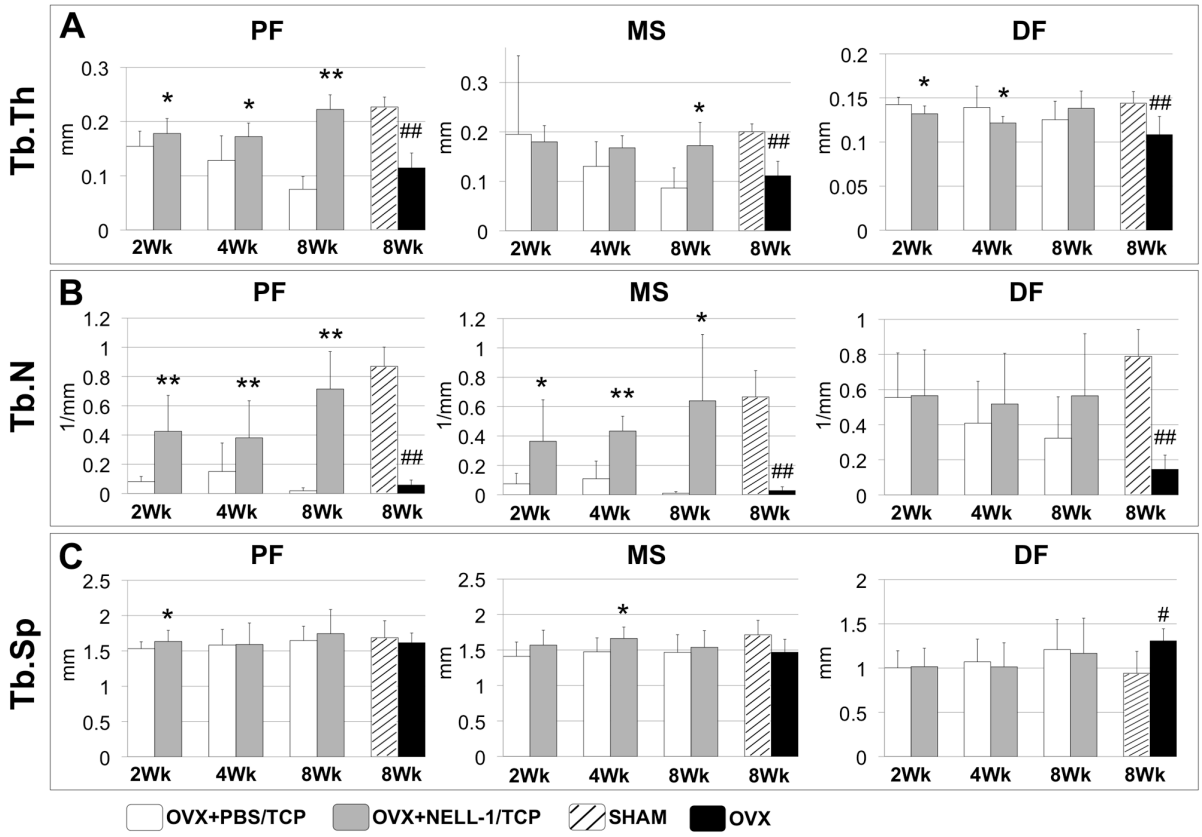

Figure 7. Quantitative microCT analysis of trabecular space, thickness, and number. The structural parameters of trabecular bone were analyzed in the PF, MS, and DF regions. The OVX+PBS/TCP control femurs at 2, 4, and 8 weeks showed a decreasing trend in (**A**) trabecular thickness (Tb.Th) and (**B**) number (Tb.N), and an increase in (**C**) trabecular spacing (Tb.S) in all three PF, MS, and DF regions. OVX+NELL-1/TCP treated femurs showed an increasing trend in Tb.Th and Tb.N, reaching SHAM levels by 8 weeks. Statistically significant increases in Tb.Th and Tb.N were found between OVX+PBS/TCP control and OVX+NELL-1/TCP femurs in PF and MS, but less in DF. The trabecular parameters in DF region appeared to be the least affected by OVX and/or treatment. * $p < 0.05$, ** $p < 0.01$ for paired t-test between PBS/TCP and NELL-

1/TCP groups within each time point; # $p < 0.05$, ## $p < 0.01$ for 1-way, unpaired t-test between SHAM and OVX groups.

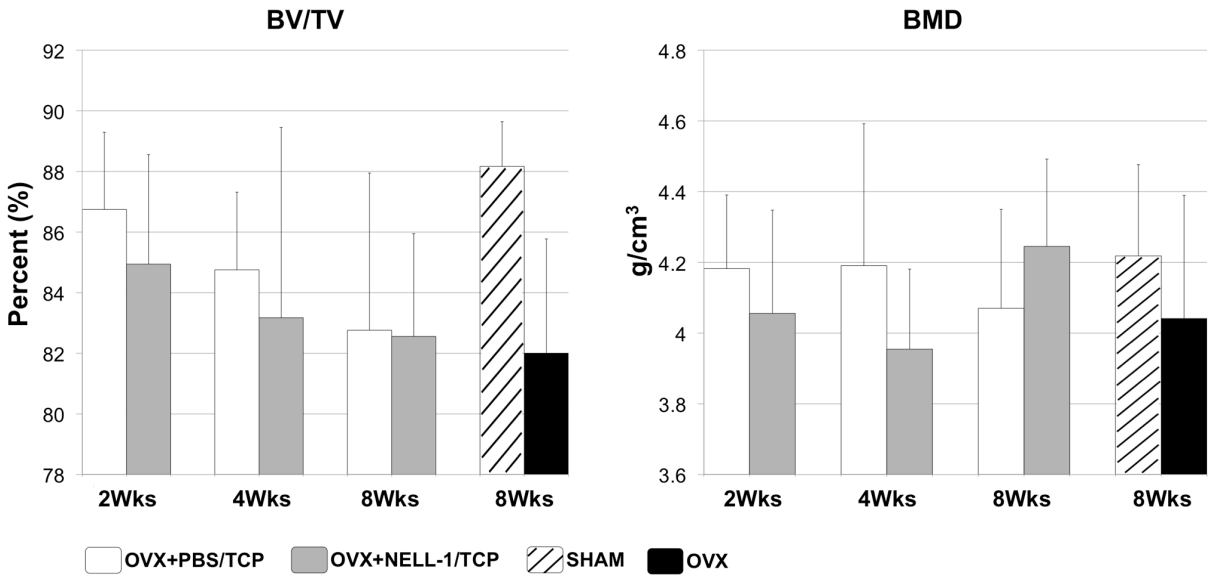

Figure 8. Quantitative microCT analysis of cortical bone volume and bone mineral density.

No statistical significance found.

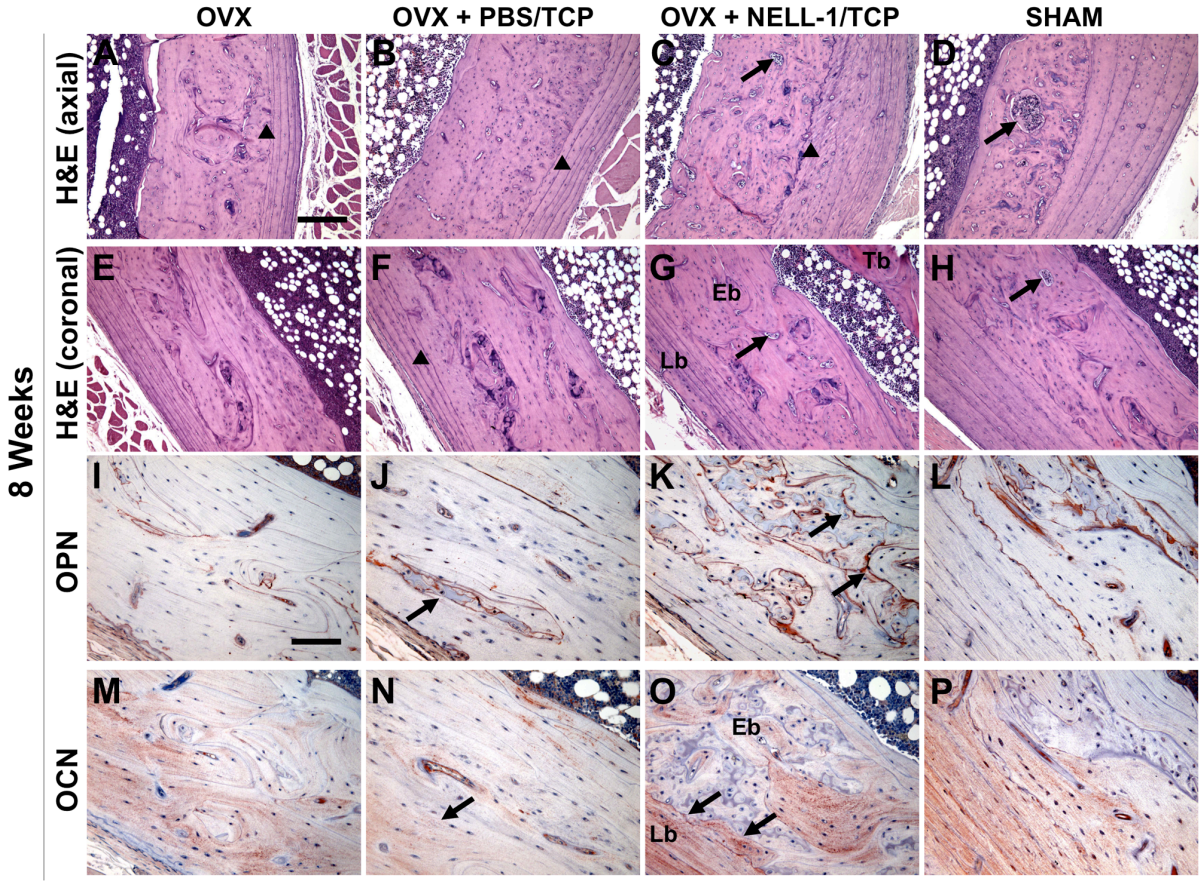

Figure 9. Histologic assessment of bone formation. Representative Hematoxylin-Eosin (HE) staining of axial mid-shaft (**A-D**) and longitudinal sections (**E-H**) of femoral bones is shown from the 8 week OVX+PBS/TCP control and OVX+NELL-1/TCP, as well as 8 week OVX only and SHAM groups. Distinct differences in morphology between NELL-1 treatment and control is evident, with increased endosteal woven bone encompassing small bone islands in OVX+NELL-1/TCP samples, indicating more active new bone formation (**arrows**). In addition, the thickness of the outer lamellar bone was increased in OVX+NELL-1/TCP samples (**arrowheads**), which is almost indistinguishable from that of SHAM control at 8 weeks. Scale bar: 200 μm for all HE images. The distribution and intensity of Osteopontin (OPN; **I-L**) and Osteocalcin (OCN; **M-P**) immunostaining were significantly enhanced in OVX+NELL-1/TCP

samples (**arrows**) indicating more active bone formation and remodeling compared to control treated samples. Scale bar: 100 µm for all immunohistochemistry images. Lb: lamellar bone; Eb: endosteal bone; Tb: trabecular bone.

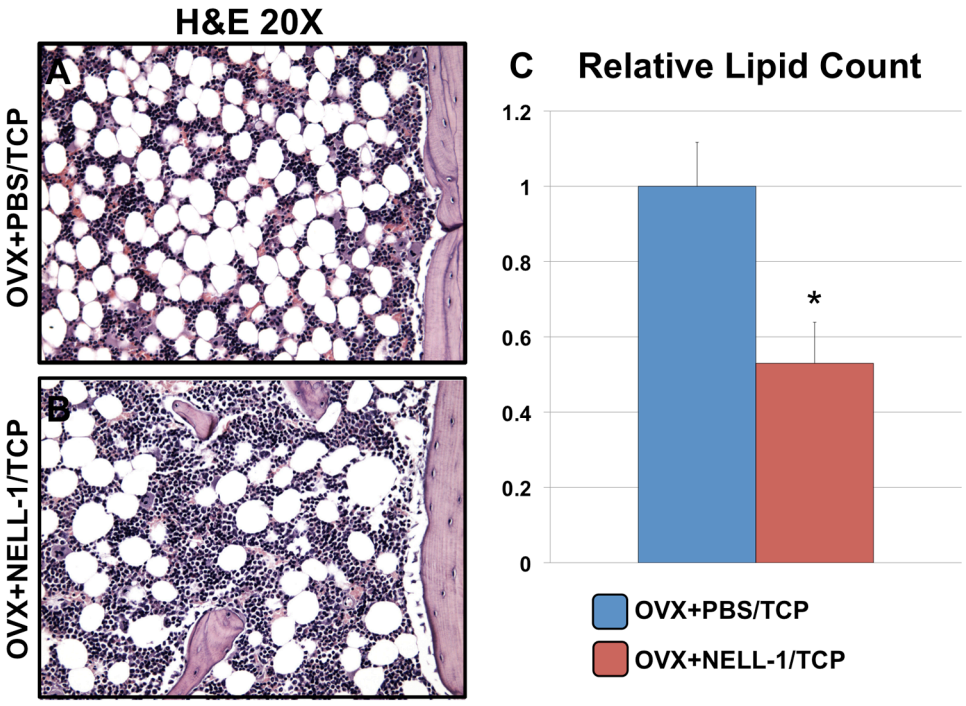

Figure 10. H&E staining showing adipocyte count. Quantification of H&E histological images of (**A**) OVX+PBS/TCP and (**B**) OVX+NELL-1/TCP femurs at 8 weeks for relative intra-marrow adiposity showed statistically significant reduction in lipid area with NELL-1 treatment (**C**). * $p < 0.05$.

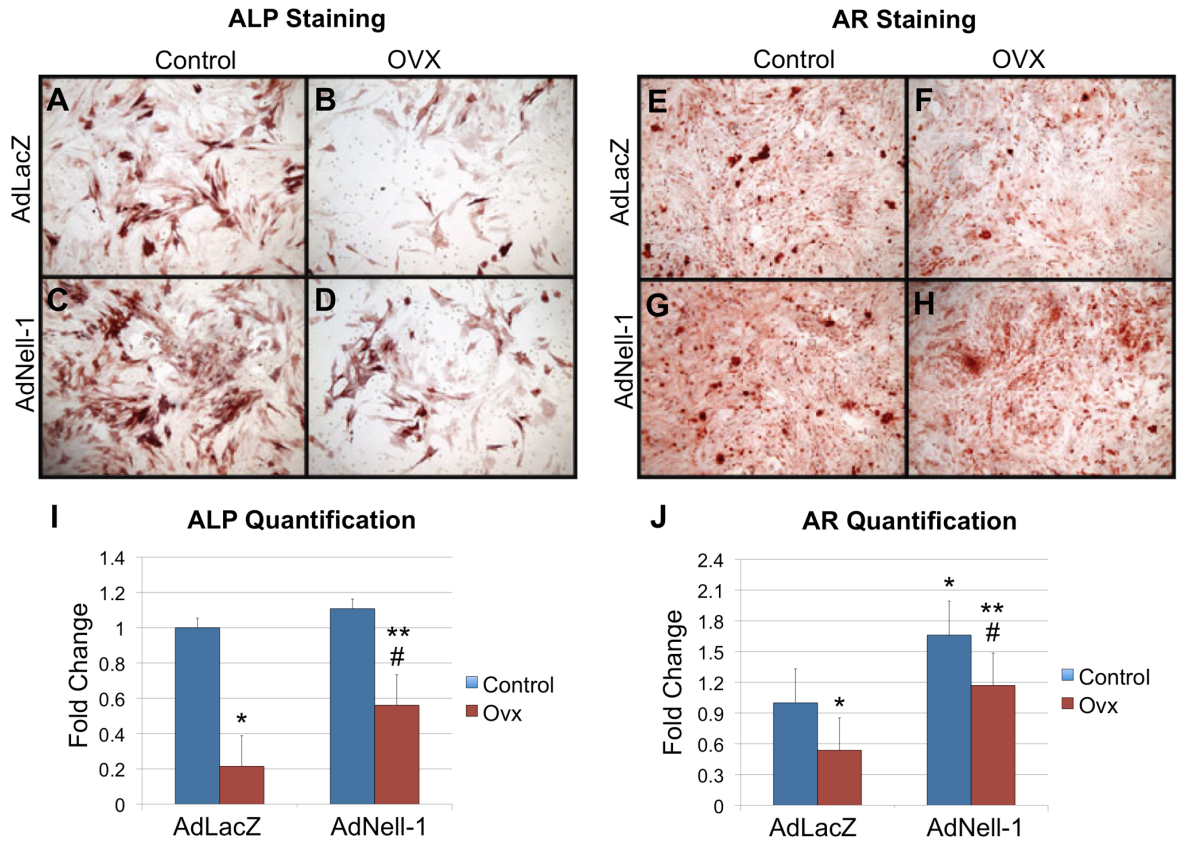

Figure 11. *In vitro* osteogenic differentiation assays. The effects of AdNell-1 on bone marrow stem cells (BMSCs) derived from healthy or OVX rats were compared. (**A-D**) Assessment of early osteogenic differentiation by alkaline phosphatase (ALP), and (**E-H**) terminal differentiation / bone nodule formation by alizarin red (AR) staining showed reduction of all markers in the OVX BMSCs at baseline. Addition of AdNell-1 increased osteogenic differentiation by both (**I**) ALP and (**J**) AR staining quantification in control and OVX BMSCs. * $p < 0.05$ with respect to Control AdLacZ, ** $p < 0.05$ with respect to Control AdNell-1, # $p < 0.05$ with respect to OVX AdLacZ.

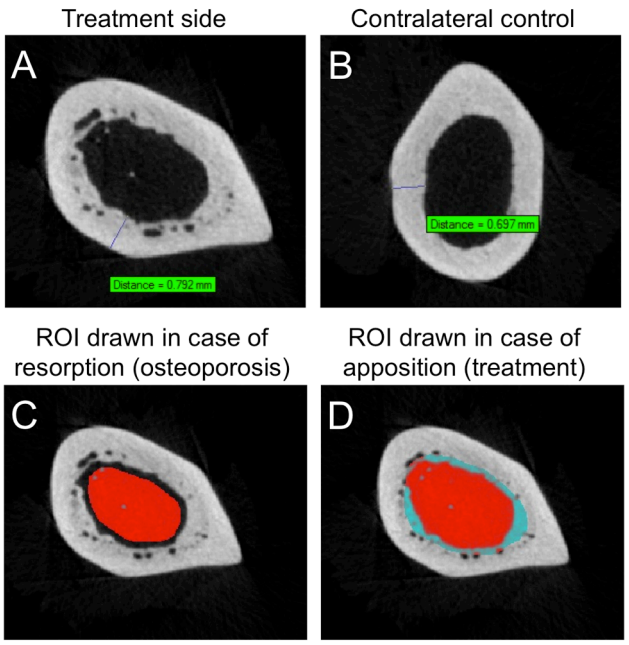

Figure 12. MicroCT verification of bone apposition or resorption.

REFERENCES

1. Giannoudis PV, Dinopoulos H, Tsiridis E. Bone substitutes: an update. Injury.36 Suppl 3:S20-7. 2005.
2. Bagaria V, Prasada V. Bone morphogenic protein: Current state of field and the road ahead. JOrthopaedics2005. pp. e3.
3. NationalOsteoporosisFoundation. Clinician's Guide to Prevention and Treatment of Osteoporosis. Washington, DC.2010.
4. Muschler GF, Nitto H, Boehm CA, Easley KA. Age- and gender-related changes in the cellularity of human bone marrow and the prevalence of osteoblastic progenitors. J Orthop Res.19:117-25. 2001.
5. Surgeon General UDoHaHS. 2004.
6. Burge RT D-HB, Solomon D, Wong JB, King AB, Tosteson ANA. Incidence and economic burden of osteoporotic fractures in the United States, 2005-2025. J Bone Min Res 22:465-75. 2007.
7. Post TM, Cremers SC, Kerbusch T, Danhof M. Bone physiology, disease and treatment: towards disease system analysis in osteoporosis. Clin Pharmacokinet.49:89-118.
8. Dominguez LJ, Di Bella G, Belvedere M, Barbagallo M. Physiology of the aging bone and mechanisms of action of bisphosphonates. Biogerontology.12:397-408.
9. Kahn A, Gibbons R, Perkins S, Gazit D. Age-related bone loss. A hypothesis and initial assessment in mice. Clin Orthop Relat Res.69-75. 1995.
10. Gimble JM, Zvonic S, Floyd ZE, Kassem M, Nuttall ME. Playing with bone and fat. J Cell Biochem.98:251-66. 2006.
11. Khan SN, Lane JM. The use of recombinant human bone morphogenetic protein-2 (rhBMP-2) in orthopaedic applications. Expert Opin Biol Ther.4:741-8. 2004.
12. Chao EY, Inoue N, Koo TK, Kim YH. Biomechanical considerations of fracture treatment and bone quality maintenance in elderly patients and patients with osteoporosis. Clin Orthop Relat Res.12-25. 2004.
13. Stromsoe K. Fracture fixation problems in osteoporosis. Injury.35:107-13. 2004.
14. Weil YA, Rivkin G, Safran O, Liebergall M, Foldes AJ. The outcome of surgically treated femur fractures associated with long-term bisphosphonate use. J Trauma.71:186-90. 2011.
15. Giannoudis P, Tzioupis C, Almalki T, Buckley R. Fracture healing in osteoporotic fractures: is it really different? A basic science perspective. Injury.38 Suppl 1:S90-9. 2007.
16. Tsolaki IN, Madianos PN, Vrotsos JA. Outcomes of dental implants in osteoporotic patients. A literature review. J Prosthodont.18:309-23. 2009.
17. Slagter KW, Raghoebar GM, Vissink A. Osteoporosis and edentulous jaws. Int J Prosthodont.21:19-26. 2008.
18. Hohlweg-Majert B, Schmelzeisen R, Pfeiffer BM, Schneider E. Significance of osteoporosis in craniomaxillofacial surgery: a review of the literature. Osteoporos Int.17:167-79. 2006.
19. Bedogni A, Bettini G, Totola A, Saia G, Nocini PF. Oral bisphosphonate-associated osteonecrosis of the jaw after implant surgery: a case report and literature review. J Oral Maxillofac Surg.68:1662-6. 2010.

20. Wang HL, Weber D, McCauley LK. Effect of long-term oral bisphosphonates on implant wound healing: literature review and a case report. J Periodontol.78:584-94. 2007.
21. Montagnani A, Gonnelli S, Alessandri M, Nuti R. Osteoporosis and risk of fracture in patients with diabetes: an update. Aging Clin Exp Res.23:84-90. 2011.
22. Kassem M, Marie PJ. Senescence-associated intrinsic mechanisms of osteoblast dysfunctions. Aging Cell.10:191-7. 2011.
23. Vahle JL, Sato M, Long GG, Young JK, Francis PC, Engelhardt JA, et al. Skeletal changes in rats given daily subcutaneous injections of recombinant human parathyroid hormone (1-34) for 2 years and relevance to human safety. Toxicol Pathol.30:312-21. 2002.
24. Tashjian AH, Jr., Gagel RF. Teriparatide [human PTH(1-34)]: 2.5 years of experience on the use and safety of the drug for the treatment of osteoporosis. J Bone Miner Res.21:354-65. 2006.
25. Sewerynek E, Stuss M. Bisphosphonates and the risk of atrial fibrillation. Endokrynol Pol.62:93-6.
26. Boraiah S, Paul O, Hawkes D, Wickham M, Lorich DG. Complications of recombinant human BMP-2 for treating complex tibial plateau fractures: a preliminary report. Clin Orthop Relat Res.467:3257-62. 2009.
27. Carragee EJ, Hurwitz EL, Weiner BK. A critical review of recombinant human bone morphogenetic protein-2 trials in spinal surgery: emerging safety concerns and lessons learned. Spine J.11:471-91.
28. Sciadini MF, Johnson KD. Evaluation of recombinant human bone morphogenetic protein-2 as a bone-graft substitute in a canine segmental defect model. J Orthop Res.18:289-302. 2000.
29. Zara JN, Siu RK, Zhang X, Shen J, Ngo R, Lee M, et al. High doses of bone morphogenetic protein 2 induce structurally abnormal bone and inflammation in vivo. Tissue Eng Part A.17:1389-99.
30. Ting K, Vastardis H, Mulliken JB, Soo C, Tieu A, Do H, et al. Human Nell-1 expressed in unilateral coronal synostosis. J Bone Miner Res.14:80-9. 1999.
31. Desai J, Shannon ME, Johnson MD, Ruff DW, Hughes LA, Kerley MK, et al. Nell1-deficient mice have reduced expression of extracellular matrix proteins causing cranial and vertebral defects. Human Molecular Genetics.15:1329-41. 2006.
32. Siu RK, Lu SS, Li W, Whang J, McNeill G, Zhang X, et al. Nell-1 Protein Promotes Bone Formation in a Sheep Spinal Fusion Model. Tissue Eng Part A.
33. Zhang X, Kuroda S, Carpenter D, Nishimura I, Soo C, Moats R, et al. Craniosynostosis in transgenic mice overexpressing Nell-1. J Clin Invest.110:861-70. 2002.
34. Thompson DD, Simmons HA, Pirie CM, Ke HZ. FDA Guidelines and animal models for osteoporosis. Bone.17:125S-33S. 1995.
35. Jee WS, Yao W. Overview: animal models of osteopenia and osteoporosis. J Musculoskelet Neuronal Interact.1:193-207. 2001.
36. Jee WS, Yao W. Animal models of bone diseases. Introduction. J Musculoskelet Neuronal Interact.1:183-4. 2001.
37. Heneweer M, Houtman R, Poortman J, Groot M, Maliepaard C, Peijnenburg A. Estrogenic effects in the immature rat uterus after dietary exposure to ethinylestradiol and zearalenone using a systems biology approach. Toxicol Sci.99:303-14. 2007.

38. Papaconstantinou AD, Umbreit TH, Fisher BR, Goering PL, Lappas NT, Brown KM. Bisphenol A-induced increase in uterine weight and alterations in uterine morphology in ovariectomized B6C3F1 mice: role of the estrogen receptor. Toxicol Sci.56:332-9. 2000.
39. Li W, Lee M, Whang J, Siu RK, Zhang X, Liu C, et al. Delivery of lyophilized Nell-1 in a rat spinal fusion model. Tissue Eng Part A.16:2861-70. 2010.
40. Parfitt AM, Drezner MK, Glorieux FH, Kanis JA, Malluche H, Meunier PJ, et al. Bone histomorphometry: standardization of nomenclature, symbols, and units. Report of the ASBMR Histomorphometry Nomenclature Committee. J Bone Miner Res.2:595-610. 1987.
41. James AW, Leucht P, Levi B, Carre AL, Xu Y, Helms JA, et al. Sonic Hedgehog influences the balance of osteogenesis and adipogenesis in mouse adipose-derived stromal cells. Tissue Eng Part A.16:2605-16.
42. James AW, Pan A, Chiang M, Zara JN, Zhang X, Ting K, et al. A new function of Nell-1 protein in repressing adipogenic differentiation. Biochem Biophys Res Commun.411:126-31.
43. Levi B, James AW, Glotzbach JP, Wan DC, Commons GW, Longaker MT. Depot-specific variation in the osteogenic and adipogenic potential of human adipose-derived stromal cells. Plast Reconstr Surg.126:822-34.
44. Ruth EB. Bone studies. II. An experimental study of the Haversian-type vascular channels. am j anat.93:429-55. 1953.
45. de Winter FR, Steendijk R. The effect of a low-calcium diet in lactating rats; observations on the rapid development and repair of osteoporosis. Calcif Tissue Res.17:303-16. 1975.
46. Li XJ JW, Ke HZ, Mori S, Akamine T. Age related changes of cancellous and cortical bone histomorphometry in female Sprague-Dawley rats. Cells Mater.(Suppl)1:25-37. 1992.
47. Schapira D L-MR, Barzilai D, Silbermann M. The rat as a model for studies of the aging skeleton. Cells Mater.(Suppl)1:181-8. 1992.
48. Steger RW, Huang HH, Chamberlain DS, Meites J. Changes in control of gonadotropin secretion in the transition period between regular cycles and constant estrus in aging female rats. Biol Reprod.22:595-603. 1980.
49. Miller BH, Gore AC. N-Methyl-D-aspartate receptor subunit expression in GnRH neurons changes during reproductive senescence in the female rat. Endocrinology.143:3568-74. 2002.
50. Seeman E. Structural basis of growth-related gain and age-related loss of bone strength. Rheumatology (Oxford).47 Suppl 4:iv2-8. 2008.
51. Truong T, Zhang X, Pathmanathan D, Soo C, Ting K. Craniosynostosis-associated gene nell-1 is regulated by runx2. J Bone Miner Res.22:7-18. 2007.
52. Bokui N, Otani T, Igarashi K, Kaku J, Oda M, Nagaoka T, et al. Involvement of MAPK signaling molecules and Runx2 in the NELL1-induced osteoblastic differentiation. FEBS Lett.582:365-71. 2008.
53. Zhang X, Ting K, Bessette CM, Culiat CT, Sung SJ, Lee H, et al. Nell-1, a key functional mediator of Runx2, partially rescues calvarial defects in Runx2(+/-) mice. J Bone Miner Res.26:777-91. 2011.
54. Egermann M, Heil P, Tami A, Ito K, Janicki P, Von Rechenberg B, et al. Influence of defective bone marrow osteogenesis on fracture repair in an experimental model of senile osteoporosis. J Orthop Res.28:798-804.
55. Xiao Y, Fu H, Prasadam I, Yang YC, Hollinger JO. Gene expression profiling of bone marrow stromal cells from juvenile, adult, aged and osteoporotic rats: with an emphasis on osteoporosis. Bone.40:700-15. 2007.

56. Chen TL. Inhibition of growth and differentiation of osteoprogenitors in mouse bone marrow stromal cell cultures by increased donor age and glucocorticoid treatment. Bone.35:83-95. 2004.
57. Li DJ, Ge DX, Wu WC, Wu J, Li L. [Osteogenic potential of bone marrow mesenchymal stem cells from ovariectomied osteoporotic rat]. Sichuan Da Xue Xue Bao Yi Xue Ban.36:318-21. 2005.
58. Gaur T, Lengner CJ, Hovhannisyan H, Bhat RA, Bodine PV, Komm BS, et al. Canonical WNT signaling promotes osteogenesis by directly stimulating Runx2 gene expression. J Biol Chem.280:33132-40. 2005.
59. Brault V, Moore R, Kutsch S, Ishibashi M, Rowitch DH, McMahon AP, et al. Inactivation of the beta-catenin gene by Wnt1-Cre-mediated deletion results in dramatic brain malformation and failure of craniofacial development. Development.128:1253-64. 2001.
60. Ross SE, Hemati N, Longo KA, Bennett CN, Lucas PC, Erickson RL, et al. Inhibition of adipogenesis by Wnt signaling. Science.289:950-3. 2000.
61. Zhou S, Eid K, Glowacki J. Cooperation between TGF-beta and Wnt pathways during chondrocyte and adipocyte differentiation of human marrow stromal cells. J Bone Miner Res.19:463-70. 2004.
62. Zhang X TK, Pathmanathan D, Ko T, Chen W, Chen F, Lee H, James AW, Siu RK, Shen J, Culiat CT, Soo C. Calvarial Cleidocraniodysplasia-like defects with ENU-Induced Nell-1 Deficiency. J Craniofac Surg. 2010.
63. Karasik D, Hsu YH, Zhou Y, Cupples LA, Kiel DP, Demissie S. Genome-wide pleiotropy of osteoporosis-related phenotypes: the Framingham Study. J Bone Miner Res.25:1555-63.
64. Zhang X, Zara J, Siu RK, Ting K, Soo C. The role of NELL-1, a growth factor associated with craniosynostosis, in promoting bone regeneration. J Dent Res.89:865-78. 2010.
65. Siu RK, Lu SS, Li W, Whang J, McNeill G, Zhang X, et al. Nell-1 protein promotes bone formation in a sheep spinal fusion model. Tissue Eng Part A.17:1123-35. 2011.
66. Lee M, Li W, Siu RK, Whang J, Zhang X, Soo C, et al. Biomimetic apatite-coated alginate/chitosan microparticles as osteogenic protein carriers. Biomaterials.30:6094-101. 2009.
67. Li W, Zara JN, Siu RK, Lee M, Aghaloo T, Zhang X, et al. Nell-1 enhances bone regeneration in a rat critical-sized femoral segmental defect model. Plast Reconstr Surg.127:580-7. 2011.